

Dynamic Optimal Transport with Mixed Boundary Conditions for Color Image Processing

Jan Henrik Fitschen, Friederike Laus and Gabriele Steidl

Department of Mathematics, University of Kaiserslautern, Germany

{fitschen, friederike.laus, steidl}@mathematik.uni-kl.de

August 1, 2018

Abstract

Recently, Papadakis et al. [12] proposed an efficient primal-dual algorithm for solving the dynamic optimal transport problem with quadratic ground cost and measures having densities with respect to the Lebesgue measure. It is based on the fluid mechanics formulation by Benamou and Brenier [2] and proximal splitting schemes. In this paper we extend the framework to color image processing. We show how the transportation problem for RGB color images can be tackled by prescribing periodic boundary conditions in the color dimension. This requires the solution of a 4D Poisson equation with mixed Neumann and periodic boundary conditions in each iteration step of the algorithm. This 4D Poisson equation can be efficiently handled by fast Fourier and Cosine transforms. Furthermore, we sketch how the same idea can be used in a modified way to transport periodic 1D data such as the histogram of cyclic hue components of images. We discuss the existence and uniqueness of a minimizer of the associated energy functional. Numerical examples illustrate the meaningfulness of our approach.

1 Introduction

Recently, methods from optimal transport (OT) have gained a lot of interest in image processing. In one of the first applications, the Wasserstein distance (earth mover distance) has been successfully used for image retrieval [19] and since then it has been applied to many other tasks as color transfer [15, 17], (co)segmentation [10, 14, 20], the synthesis and mixing of stationary Gaussian textures [1] and the computation of barycenters [18, 8].

The basic problem, going back to Monge (1746-1818), can be formulated as follows: Given two probability spaces (\mathcal{X}, μ_0) and (\mathcal{Y}, μ_1) and a nonnegative cost function $c(x, y)$ on $\mathcal{X} \times \mathcal{Y}$, find a transport map $T: \mathcal{X} \rightarrow \mathcal{Y}$ that transports the mass of μ_0 to the mass of μ_1 at minimal cost, i.e., T minimizes

$$\int_{\mathcal{X}} c(x, T(x)) d\mu_0(x) \quad \text{subject to} \quad \mu_0 \circ T^{-1} = \mu_1. \quad (1)$$

One of the major limitations in applications using OT is the fact that it is in general not known whether a solution of problem (1) exists and even in this

case the computation of the optimal map T is usually a demanding task (except very few cases, e.g. OT on \mathbb{R} with convex costs). We focus in the following on a specific instance of problem (1), namely if $\mathcal{X} = \mathcal{Y} = \mathbb{R}^d$, $c(x, y) = \frac{1}{2} |x - y|^2$ and μ_0 and μ_1 are absolutely continuous w.r.t. the Lebesgue measure, that means there exist probability density functions f^0 and f^1 with

$$\mu_i(A) = \int_A f^i(x) dx, \quad i = 0, 1, \quad A \in \mathcal{B}(\mathbb{R}^d).$$

In this case there exists a unique optimal transport map T that transports f^0 to f^1 , see, e.g., [6, 21]. Instead of considering a time independent, “static” mass transportation problem one may alternatively consider the geodesic path between the two measures w.r.t. to the Wasserstein metric (the so called displacement interpolation [9]). While the static problem can be seen as a distance problem (find the minimal distance between the probability measures μ_0 and μ_1), the dynamic problem can be interpreted as a geodesic problem (find an optimal path between μ_0 and μ_1). For the L^2 ground cost this geodesic is obtained by linear interpolation between the identity and the optimal transport map T , i.e., $\mu_t = \mu_0 \circ T_t^{-1}$, where $T_t = (1 - t) \text{Id} + tT$. Benamou and Brenier [2] gave the following equivalent formulation of the dynamic OT problem in terms of fluid mechanics: minimize

$$\int_{[0,1]} \int_{\mathbb{R}^d} \frac{1}{2} f(x, t) |v(x, t)|^2 dx dt, \quad (2)$$

subject to $\bigcup_{t \in [0,1]} \text{supp } f(\cdot, t)$ bounded, $f(\cdot, 0) = f^0, f(\cdot, 1) = f^1$ and $\partial_t f + \text{div}_x(fv) = 0$, (f, v) sufficiently smooth. Substituting $m = fv$, this problem becomes convex and can be treated by respective algorithms.

In addition to the Dirichlet boundary condition for the time interval, problem (2) needs to be equipped with spatial boundary conditions in practical applications (appearing in the momentum variable m). A natural choice which was also used in [12] for gray-value images are Neumann boundary conditions. In this paper we want to deal with color RGB (red, green, blue) images. More precisely, we consider a $m \times n$ RGB image as a 3D object of size $m \times n \times 3$ with the color values in the third dimension, i.e., we interpret these images as (realization of) a 3D density function. To use Neumann boundary conditions for the color dimension is certainly not a good idea since the solution can depend on the ordering of the color channels. Therefore, we suggest to establish periodic boundary conditions in the third dimension. Note that we have Dirichlet boundary conditions in time, and Neumann plus periodic spatial boundary conditions. Fig. 1 illustrates the effect of the different boundary conditions. In Section 2 we explain the discretization of problem (2) emphasizing the mixed boundary conditions. In particular we deal with the existence and uniqueness of minimizers. Similarly as suggested in [12] we apply a primal dual algorithm to find a minimizer in Section 3. In contrast to [12] each iteration step of this algorithm requires the solution of a 4D Poisson problem with mixed Neumann and periodic boundary conditions which can be efficiently computed by applying FFTs and fast cosine transforms. In Section 4 we apply our findings to the dynamic OT of RGB images which was the initial motivation of this work. Another application is given in Section 5. Here, the (cyclic) OT is applied to HSV (hue, saturation, value) images, where only the cyclic hue component is transported. For further details we refer to [7].

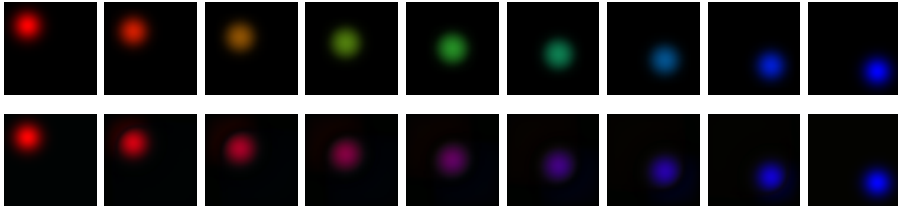


Figure 1: OT results for transporting a red Gaussian into a blue one with different boundary conditions for the third (color) dimension. First row: Neumann boundary conditions; the color is transported from red over green to blue. This changes if we permute the RGB channels. Second row: periodic boundary conditions; the color is transported from red over violet to blue which is more intuitive and does not change for permuted color channels.

2 Model for dynamic OT with mixed boundaries

Rewriting (2) for $m = fv$, we see that the geodesic path between measures with probability densities $f^0 = f(\cdot, 0)$ and $f^1 = f(\cdot, 1)$ has density $f(\cdot, t)$ fulfilling

$$\operatorname{argmin}_{(m,f) \in \mathcal{C}} \int_{[0,1]} \int_{[0,1]^d} J(m, f) \, dx \, dt, \quad (3)$$

where

$$J(m(x, t), f(x, t)) := \begin{cases} \frac{|m(x, t)|^2}{2f(x, t)} & \text{if } f(x, t) > 0, \\ 0 & \text{if } (m(x, t), f(x, t)) = (0_d^T, 0), \\ +\infty & \text{otherwise,} \end{cases}$$

$$\mathcal{C} := \{(f, m) : \partial_t f + \operatorname{div}_x m = 0, f(\cdot, 0) = f^0, f(\cdot, 1) = f^1\}$$

with appropriate boundary conditions. In the following, we describe the discretization of problem (3) for one spatial dimension with cyclic spatial boundary conditions. The discretization of the continuity equation demands the evaluation of discrete partial derivatives in time as well as in space. In order to avoid solutions suffering from the well-known checkerboard-effect (see for instance [13]) we adopt the idea of a staggered grid as in [12].

Discretization (Spatial 1D): We consider the values of f at spatial cell mid-points $\frac{j-1/2}{n}$, $j = 1, \dots, n$ and time $\frac{k}{p}$, $k = 1, \dots, p-1$, and denote the corresponding array by $(f(j - \frac{1}{2}, k))_{j=1, k=1}^{n, p-1} \in \mathbb{R}^{n, p-1}$. The boundary values are assumed to be fixed in $f^0 := (f(\frac{j-1/2}{n}, 0))_{j=1}^n$ and $f^1 := (f(\frac{j-1/2}{n}, 1))_{j=1}^n$, where $f^i \geq 0$, $i = 0, 1$ and $\|f^0\|_1 = \|f^1\|_1$. We can skip the normalization $\|f^0\|_1 = 1$ here. The values of m are taken at the cell faces $\frac{j}{n}$, $j = \kappa, \dots, n-1$ and time $\frac{k-1/2}{p}$, $k = 1, \dots, p$ and we consider the array $(m(j, k - \frac{1}{2}))_{j=\kappa, k=1}^{n-1, p} \in \mathbb{R}^{n-\kappa, p}$, where $\kappa = 1$ for Neumann boundary conditions and $\kappa = 0$ for periodic boundary conditions, see Fig. 2. To give a sound matrix-vector notation of the discrete minimization problem we reorder m and f columnwise into vectors $f = \operatorname{vec}(f) \in$

$\mathbb{R}^{n(p-1)}$, $m = \text{vec}(m) \in \mathbb{R}^{(n-\kappa)p}$. Since it becomes clear from the context if we deal with arrays or vectors we use the same notation. The derivatives in \mathcal{C} are approximated by forward differences and the integral in (3) by a midpoint rule, where the midpoints $(u(j - \frac{1}{2}, k - \frac{1}{2}))_{j,k=1}^{n,p}$ and $(v(j - \frac{1}{2}, k - \frac{1}{2}))_{j,k=1}^{n,p}$ are computed by averaging the neighboring two values. This results in the following

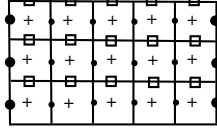


Figure 2: Discretization grid for the dynamic OT problem for 1D signals f : horizontal direction for time; vertical direction for space; • given boundary sampling nodes f^0 and f^1 , · sampling nodes for $f((j-1/2)/n, k)$, $j = 1, \dots, n$, $k = 1, \dots, p-1$, □ sampling nodes for m , '+' quadrature nodes.

discrete model:

$$\underset{m, f, u, v}{\text{argmin}} \|J(u, v)\|_1, \quad (4)$$

$$\text{subject to } S_M m = u, \quad S_F f + f_b^+ = v,$$

$$\underbrace{(D_M | D_F)}_A \begin{pmatrix} m \\ f \end{pmatrix} = f_b^-. \quad (5)$$

We denote

$$\mathcal{C}_d := \left\{ \begin{pmatrix} m \\ f \end{pmatrix} \in \mathbb{R}^{(n-\kappa)p+n(p-1)} : (D_M | D_F) \begin{pmatrix} m \\ f \end{pmatrix} = f_b^- \right\}.$$

The involved vectors are defined as

$$f_b^+ := \frac{1}{2} ((f^0)^\top, 0_{n(p-2)}, (f^1)^\top)^\top,$$

$$f_b^- := p((f^0)^\top, 0_{n(p-2)}, -(f^1)^\top)^\top$$

and the matrices using the Kronecker product \otimes as

$$S_F := S_p^\top \otimes I_n, \quad D_F := -D_p^\top \otimes I_n,$$

$$S_M := \begin{cases} I_p \otimes S_n^\top & \text{Neumann,} \\ I_p \otimes S_{n,per}^\top & \text{periodic,} \end{cases} \quad D_M := \begin{cases} I_p \otimes -D_n^\top & \text{Neumann,} \\ I_p \otimes D_{n,per}^\top & \text{periodic,} \end{cases}$$

and

$$S_{n,per} := \frac{1}{2} \begin{pmatrix} 1 & 0 & & & & 1 \\ 1 & 1 & & & & \\ & & \ddots & & & \\ & & & 1 & 1 & 0 \\ & & & & 1 & 1 \end{pmatrix} \in \mathbb{R}^{n,n},$$

$$S_p := \frac{1}{2} \begin{pmatrix} 1 & 1 & 1 & & & \\ & & & \ddots & & \\ & & & & 1 & 1 \end{pmatrix} \in \mathbb{R}^{p-1,p},$$

$$D_{n,per} := n \begin{pmatrix} -1 & & & 1 \\ 1 & -1 & & \\ & & \ddots & \\ & & & -1 & 0 \\ & & & 1 & -1 \end{pmatrix} \in \mathbb{R}^{n,n},$$

$$D_p := p \begin{pmatrix} -1 & & & 1 \\ 1 & -1 & & \\ & & \ddots & \\ & & & -1 & 1 & 0 \\ & & & & -1 & 1 \end{pmatrix} \in \mathbb{R}^{p-1,p}.$$

Since we have to be slightly careful concerning the uniqueness of the solution in the periodic setting we provide the following proposition.

Theorem 1. *The discrete dynamic transport model (4) has a solution.*

Proof. For periodic boundary conditions and even n , we have $\mathcal{N}(S_M) = \{w \otimes \tilde{1}_n : w \in \mathbb{R}^p\}$ with $\tilde{1}_n := (1, -1, \dots, 1, -1)^T \in \mathbb{R}^n$, and $\mathcal{N}(S_M) = \{0_{np}\}$ otherwise. The constraints in \mathcal{C}_d can be rewritten as

$$D_F f = f_b^- - D_M m, \quad f = D_F^\dagger f_b^- - D_F^\dagger D_M m$$

with the Moore-Penrose inverse $D_F^\dagger = (D_F^T D_F)^{-1} D_F^T$. Then we obtain

$$\operatorname{argmin}_{u,v} \|J(u,v)\|_1 = \operatorname{argmin}_m \|J(X(m), Y(m))\|_1$$

with $X(m) := S_M m$, $Y(m) := -S_F D_F^\dagger D_M m + S_F D_F^\dagger f_b^- + f_b^+$. Let $\|m\|_2 \rightarrow +\infty$ and assume that $\|J(X(m), Y(m))\|_1$ is bounded. Then each of the quotients is bounded, i.e., there exists $c > 0$ such that $X(m)_i^2 \leq c|Y(m)_i|$ and therefore $\|X(m)\|_2^2 \leq c\|Y(m)\|_1$. Thus, in the case $\mathcal{N}(S_M) = \{0_{np}\}$, we get

$$(1/\|S_M^\dagger\|_2^2) \|m\|_2^2 \leq \|X(m)\|_2^2 \leq c\|Y(m)\|_1 \tag{6}$$

$$\leq c\|S_F D_F^\dagger D_M\|_1 \|m\|_1 + \bar{c},$$

which is not possible as $\|m\|_2 \rightarrow +\infty$. In the case $\mathcal{N}(S_M) = \{w \otimes \tilde{1}_n : w \in \mathbb{R}^p\}$ we use the orthogonal splitting $m = m_R + w \otimes \tilde{1}_n$, where $m_R \in \mathcal{R}(S_M^T)$. Straightforward computation shows that $S_F D_F^\dagger D_M (w \otimes \tilde{1}_n) = \tilde{w} \otimes \tilde{1}_n$ with some $\tilde{w} \in \mathbb{R}^p$. Since $Y(m) \geq 0$, we conclude

$$\| -S_F D_F^\dagger D_M m_R + S_F D_F^\dagger f_b^- + f_b^+ \|_\infty \geq \|\tilde{w} \otimes \tilde{1}_n\|_\infty. \tag{7}$$

If m_R remains finite, then $\tilde{1}_N \otimes \tilde{w}$ remains finite as well. Since the kernel of $S_f D_f^\dagger D_m$ consists of constant vectors, this is only possible if w is a multiple of 1_P . But in this case $J_p(X(m), Y(m))$ has a finite value which is reached. It remains to consider the case $\|m_R\|_2 \rightarrow +\infty$. Then we obtain similarly as in (6) that

$$(1/\|S_M^\dagger|_{\mathcal{R}(S_M^T)}\|_2^2) \|m_R\|_2^2 \leq \|X(m_R)\|_2^2 \leq c\|Y(m)\|_1$$

$$\leq c\| -S_F D_F^\dagger D_M m_R + S_F D_F^\dagger f_b^- + f_b^+ \|_1 + c\|\tilde{w} \otimes \tilde{1}_n\|_1.$$

By (7) we see that this is not possible as $\|m_R\|_2 \rightarrow +\infty$. In summary, we have that $\|J(X(m), Y(m))\|_1$ is coercive and since it is also proper and lower semi-continuous, it has a minimizer. \square

Unfortunately, $J(m, f)$ is not strongly convex on its domain. As it can be seen in the following lemma it is even not strictly convex.

Lemma 1. *For any two minimizers (m_i, f_i) , $i = 1, 2$ the relation*

$$\frac{S_M m_1}{S_F f_1 + f_b^-} = \frac{S_M m_2}{S_F f_2 + f_b^-}$$

holds true.

Proof. The function $J(u, v)$ is the perspective function of the strictly convex function $\psi = |\cdot|^2$, i.e., $J(u, v) = v\psi\left(\frac{u}{v}\right)$, see, e.g., [5]. For $\lambda \in (0, 1)$ and (u_i, v_i) with $v_i > 0$, $i = 1, 2$, we have (componentwise)

$$\begin{aligned} J(\lambda(u_1, v_1) + (1 - \lambda)(u_2, v_2)) &= (\lambda v_1 + (1 - \lambda)v_2) \psi\left(\frac{\lambda u_1 + (1 - \lambda)u_2}{\lambda v_1 + (1 - \lambda)v_2}\right) \\ &= (\lambda v_1 + (1 - \lambda)v_2) \psi\left(\frac{\lambda v_1}{\lambda v_1 + (1 - \lambda)v_2} \frac{u_1}{v_1} + \frac{(1 - \lambda)v_2}{\lambda v_1 + (1 - \lambda)v_2} \frac{u_2}{v_2}\right) \end{aligned}$$

and if $\frac{u_1}{v_1} \neq \frac{u_2}{v_2}$ by the strict convexity of ψ ,

$$J(\lambda(u_1, v_1) + (1 - \lambda)(u_2, v_2)) < \lambda J(u_1, v_1) + (1 - \lambda)J(u_2, v_2),$$

which proves the assertion. \square

Remark 1. *For periodic boundary conditions, even n and $f^1 = f^0 + \gamma \tilde{1}_n$, $\gamma \in [0, \min f^0]$ the minimizer of (4) is not unique which can be seen as follows: obviously, we would have a minimizer (m, f) if $m = w \otimes \tilde{1}_n \in \mathcal{N}(S_M)$ for some $w \in \mathbb{R}^p$ and there exists $f \geq 0$ which fulfills the constraints. Setting $f^{k/p} := f(j - 1/2, k)_{j=1}^n$, $k = 0, \dots, p$, these constraints read $-2pw \otimes \tilde{1}_n = p(f^{(k-1)/p} - f^{k/p})_{k=1}^p$. Thus, any $w \in \mathbb{R}^p$ such that*

$$\begin{aligned} f^{1/p} &= f^0 + 2w_1 \tilde{1}_n, \quad f^{2/p} = f^0 + 2(w_1 + w_2) \tilde{1}_n, \dots, \\ f^1 &= f^0 + 2(w_1 + w_2 + \dots + w_p) \tilde{1}_n \end{aligned}$$

are nonnegative vectors provides a minimizer of (4). We conjecture that the solution is unique in all other cases, but have no proof so far.

3 Minimization Algorithm

We apply the primal-dual algorithm of Chambolle and Pock [4] in the form of Algorithm 8 in [3]. **Step 1** requires the projection of

$$a := \begin{pmatrix} m^{(r)} \\ f^{(r)} \end{pmatrix} - \tau\sigma \begin{pmatrix} S_M^T & 0 \\ 0 & S_F^T \end{pmatrix} \begin{pmatrix} \bar{b}_m^{(r)} \\ \bar{b}_f^{(r)} \end{pmatrix}$$

onto \mathcal{C}_d which is given by

$$\begin{aligned} \Pi_{\mathcal{C}_d}(a) &= a - A^T(AA^T)^\dagger(Aa - f_b^-), \\ (AA^T)^\dagger &= Q \operatorname{diag}(\tilde{\lambda}_j) Q^T, \end{aligned}$$

Algorithm 1: PDHG Algorithm for solving (4)

Initialization: $m^{(0)} = 0_{np}$, $f^{(0)} = 0_{n(p-1)}$, $b_m^{(0)} = b_f^{(0)} = \bar{b}_m^{(0)} = \bar{b}_f^{(0)} = 0_{np}$,
 $\theta = 1$, τ, σ with $\tau\sigma < 1$.

Iteration: For $r = 0, 1, \dots$ iterate

1. $\begin{pmatrix} m^{(r+1)} \\ f^{(r+1)} \end{pmatrix} := \operatorname{argmin}_{(m,f) \in \mathcal{C}_d} \frac{1}{2\tau} \left\| \begin{pmatrix} m \\ f \end{pmatrix} - \begin{pmatrix} m^{(r)} \\ f^{(r)} \end{pmatrix} + \tau\sigma \begin{pmatrix} S_M^T & 0 \\ 0 & S_F^T \end{pmatrix} \begin{pmatrix} \bar{b}_m^{(r)} \\ \bar{b}_f^{(r)} \end{pmatrix} \right\|_2^2$
 2. $\begin{pmatrix} u^{(r+1)} \\ v^{(r+1)} \end{pmatrix} := \operatorname{argmin}_{u,v} \|J(u,v)\|_1 + \frac{\sigma}{2} \left\| \begin{pmatrix} u \\ v \end{pmatrix} - \begin{pmatrix} S_M & 0 \\ 0 & S_F \end{pmatrix} \begin{pmatrix} m^{(r+1)} \\ f^{(r+1)} \end{pmatrix} - \begin{pmatrix} 0 \\ f_b^+ \end{pmatrix} - \begin{pmatrix} b_m^{(r)} \\ b_f^{(r)} \end{pmatrix} \right\|_2^2$
 3. $b_m^{(r+1)} := b_m^{(r)} + S_M m^{(r+1)} - u^{(r+1)}$
 $b_f^{(r+1)} := b_f^{(r)} + S_F f^{(r+1)} + f_b^+ - v^{(r+1)}$
 4. $\bar{b}_m^{(r+1)} := b_m^{(r+1)} + \theta(b_m^{(r+1)} - b_m^{(r)})$
 $\bar{b}_f^{(r+1)} := b_f^{(r+1)} + \theta(b_f^{(r+1)} - b_f^{(r)})$
-

where AA^T has the spectral decomposition $AA^T = Q \operatorname{diag}(\lambda_j) Q^T$ and $\tilde{\lambda}_j := 1/\lambda_j$ if $\lambda_j > 0$ and zero otherwise. For A in (5) the application of $(AA^T)^\dagger$ requires the solution of a 2D Poisson equation. In case of periodic boundary conditions we get

$$\begin{aligned} AA^T &= I_p \otimes D_{n,per}^T D_{n,per} + D_p^T D_p \otimes I_n \\ &= I_p \otimes n^2 \Delta_{n,per} + p^2 \Delta_p \otimes I_n, \end{aligned}$$

where

$$\begin{aligned} \Delta_{n,per} &:= \begin{pmatrix} 2 & -1 & & & & -1 \\ -1 & 2 & -1 & & & \\ & & & \ddots & & \\ & & & & -1 & 2 & -1 \\ -1 & & & & -1 & -1 & 2 \\ & & & & & & \end{pmatrix}, \\ \Delta_p &:= \begin{pmatrix} 1 & -1 & & & & 0 \\ -1 & 2 & -1 & & & \\ & & & \ddots & & \\ 0 & & & & -1 & 2 & -1 \\ & & & & -1 & -1 & 1 \end{pmatrix}. \end{aligned}$$

Since

$$\Delta_{n,per} = \frac{1}{n} \bar{F}_n \operatorname{diag}(q_{n,per}) F_n, \quad q_{n,per} := \left(4 \sin^2 \frac{j\pi}{n} \right)_{j=0}^{n-1}$$

with the Fourier matrix $F_n := (e^{-2\pi ijk})_{j,k=0}^{n-1}$ and

$$\Delta_p = C_p^T \operatorname{diag}(q_p) C_p, \quad q_p := \left(4 \sin^2 \frac{j\pi}{2p} \right)_{j=0}^{p-1}$$

with the DCT-II matrix

$$C_p := \sqrt{\frac{2}{p}} \left(\epsilon_j \cos \frac{j(2k+1)\pi}{2p} \right)_{j,k=0}^{p-1}, \quad \epsilon_j := \begin{cases} 1/\sqrt{2} & \text{if } j = 0, \\ 1 & \text{otherwise} \end{cases}$$

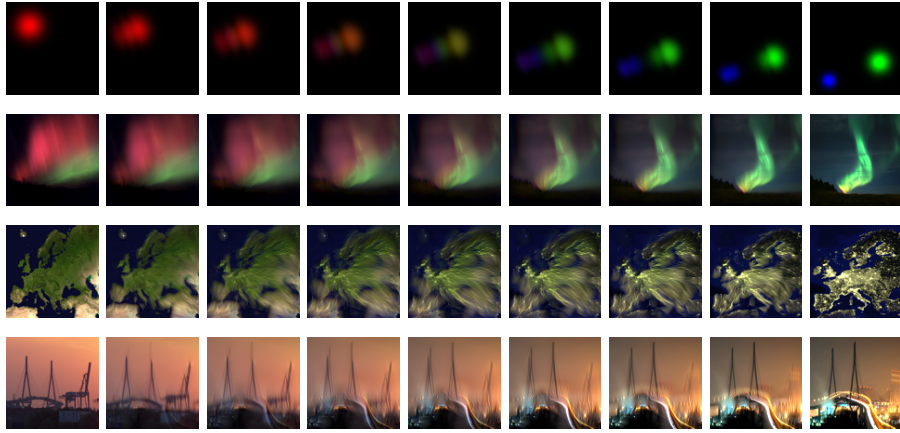


Figure 3: OT between RGB images. The images are displayed at intermediate time $t = \frac{i}{8}, i = 0, \dots, 8$.

we obtain

$$AA^T = (C_p^T \otimes \frac{1}{n} \bar{F}_n) (n^2 I_p \otimes \text{diag}(q_{n,per}) + p^2 (\text{diag}(q_p) \otimes I_n) (C_p \otimes F_n),$$

so that its pseudo-inverse can be computed by the FFT and the fast cosine transform.

Remark 2. For the transport of general 2D RGB images we have analogously to solve a 4D Poisson equation with Neumann boundary conditions and a periodic boundary condition for the color channels.

Step 2 of the algorithm can be computed componentwise as proposed in [12]. Setting $a_m := S_M m^{(r+1)} + b_m^{(r)}$, $a_f := S_F f^{(r+1)} + b_f^{(r)} + f_b^+$ we have to find componentwise

$$\underset{u,v}{\text{argmin}} \frac{u^2}{2v} + \frac{\sigma}{2} (u - a_m)^2 + \frac{\sigma}{2} (v - a_f)^2.$$

Setting the gradient to zero yields

$$\frac{u}{v} + \sigma(u - a_m) = 0, \quad -\frac{1}{2} \frac{u^2}{v^2} + \sigma(v - a_f) = 0.$$

Thus,

$$u = \frac{\sigma v a_m}{1 + \sigma v}$$

and v is the solution of the third order equation

$$f(v) = 2(1 + \sigma v)^2 (v - a_f) - \sigma a_m^2 = 0.$$

This can be solved by few Newton steps which can be computed simultaneously for all components. Alternatively, one may use Cardan's formula.



Figure 4: OT between hue histograms and histogram specification at time $t = \frac{i}{8}$, $i = 0, \dots, 8$.

4 RGB Image Transport

In our first experiment we consider the periodic color OT between two RGB images u_0 and u_1 that are used as densities f^0 and f^1 respectively. At this point it is important to choose image pairs which have approximately the same mass (i.e. the overall sum of all pixels and color channels) as one needs to rescale the images such that $\|f^0\|_1 = \|f^1\|_1$. The results of four different examples are shown in Fig. 3. The first row shows an artificial example of the transport between one red Gaussian into a blue and a green Gaussian with smaller variance. In the second row, two polar lights of different color and shape are transported into each other. The third row illustrates how a topographic map of Europe is transported into a satellite image of Europe at night. Finally, the last row displays the transport between two cranes in Hamburg. All images are of size $100 \times 100 \times 3$ and in each case, we used $P = 32$ time steps and 2000 iterations in our algorithm. Note that, however, already after 200 iterations there are no visible changes any longer. The images are depicted at intermediate times $t = \frac{i}{8}$, $i = 0, \dots, 8$. In all cases one nicely sees a continuous change of color and shape during the transport.

5 Hue Histogram Transport

In this section we perform color OT in the HSV space. We assume the final and target image have the same saturation and value such that only the cyclic hue component has to be transported: Assume we are given two images u_i , $i = 0, 1$ which differ only in the hue component represented by their normalized histograms h^i as empirical densities f^i , $i = 0, 1$. As the hue component is periodic, this fits into our setting. The intermediate histograms h^t , $t \in (0, 1)$ are then used to obtain the hue images via histogram specification. Together with the original saturation and intensity they yield the images u_t , $t \in (0, 1)$. For the histogram specification of periodic data we have applied the analysis in [16] and the exact histogram specification method for real-valued data proposed, e.g., in [11]. Fig. 4 shows an example, where the histogram of the hue component of a yellow flower is transported into the one of a red flower. The color changes gradually and in a realistic way which would not be the case if the periodicity of the hue histogram is not taken into account.

Acknowledgement: Funding by the DFG within the Research Training Group 1932 is gratefully acknowledged.

*All images from Wikimedia Commons: AGOModra_aurora.jpg by Comenius University under CC BY SA 3.0, Aurora-borealis_andoya.jpg by M. Buschmann under CC BY 3.0, Europe_satellite_orthographic.jpg and Earthlights_2002.jpg by NASA, Köhlbrandbrücke5478.jpg by G. Ries under CC BY SA 2.5, Köhlbrandbrücke.jpg by HafenCity1 under CC BY 3.0.

References

- [1] Synthesizing and mixing stationary Gaussian texture models. *SIAM Journal on Imaging Sciences*, 7(1):476–508, 2014.
- [2] J.-D. Benamou and Y. Brenier. A computational fluid mechanics solution to the Monge-Kantorovich mass transfer problem. *Numerische Mathematik*, 84(3):375–393, 2000.
- [3] M. Burger, A. Sawatzky, and G. Steidl. First order algorithms in variational image processing. *ArXiv-Preprint 1412.4237*, 2014.
- [4] A. Chambolle and T. Pock. A first-order primal-dual algorithm for convex problems with applications to imaging. *Journal of Mathematical Imaging and Vision*, 40(1):120–145, 2011.
- [5] B. Dacorogna and P. Maréchal. The role of perspective functions in convexity, polyconvexity, rank-one convexity and separate convexity. *Journal of Convex Analysis*, 15(2):271–284, 2008.
- [6] W. Gangbo and R. J. McCann. The geometry of optimal transportation. *Acta Mathematica*, 177(2):113–161, 1996.
- [7] F. Laus. *Optimal Transport and Applications in Image Processing*. Master Thesis, University of Kaiserslautern, 2015.
- [8] J. Maas, M. Rumpf, C.-B. Schönlieb, and S. Simon. A generalized model for optimal transport of images including dissipation and density modulation. *Preprint*, 2014.
- [9] R. J. McCann. A convexity principle for interacting gases. *Advances in Mathematics*, 128(1):153–179, 1997.
- [10] K. Ni, X. Bresson, T. Chan, and S. Esedoglu. Local histogram based segmentation using the Wasserstein distance. *International Journal of Computer Vision*, 84(1):97–111, 2009.
- [11] M. Nikolova and G. Steidl. Fast ordering algorithm for exact histogram specification. *IEEE Transactions on Image Processing*, 23(12):5274 – 5283, 2014.
- [12] N. Papadakis, G. Peyré, and E. Oudet. Optimal transport with proximal splitting. *SIAM Journal on Imaging Sciences*, 7(1):212–238, 2014.
- [13] S. Patankar. *Numerical Heat Transfer and Fluid Flow*. CRC Press, 1980.
- [14] G. Peyré, J. Fadili, and J. Rabin. Wasserstein active contours. In *19th IEEE ICIP*, pages 2541–2544, 2012.
- [15] F. Pitié and A. C. Kokaram. The linear Monge-Kantorovitch linear colour mapping for example-based colour transfer. *IET Conference Proceedings*, pages 23–23(1), 2007.
- [16] J. Rabin, J. Delon, and Y. Gousseau. Transportation distances on the circle. *Journal of Mathematical Imaging and Vision*, 41(1-2):147–167, 2011.

- [17] J. Rabin and G. Peyré. Wasserstein regularization of imaging problem. In *18th IEEE ICIP*, pages 1541–1544, 2011.
- [18] J. Rabin, G. Peyré, J. Delon, and M. Bernot. Wasserstein barycenter and its application to texture mixing. In *SSVM*, pages 435–446. Springer, 2012.
- [19] Y. Rubner, C. Tomasi, and L. J. Guibas. The earth mover’s distance as a metric for image retrieval. *International Journal of Computer Vision*, 40(2):99–121, 2000.
- [20] P. Swoboda and C. Schnörr. Convex variational image restoration with histogram priors. *SIAM Journal on Imaging Sciences*, 6(3):1719–1735, 2013.
- [21] C. Villani. *Topics in Optimal Transportation*. AMS, Providence, 2003.